

PREPARED FOR SUBMISSION TO JHEP

Condensates in Relativistic Scalar Theories

Guy D. Moore

*Institut für Kernphysik, Technische Universität Darmstadt
Schlossgartenstraße 2, D-64289 Darmstadt, Germany*

ABSTRACT: Scalar field theory with large infrared initial occupancy develops very large deep-infrared occupancy, which locally resembles a Bose-Einstein condensate. We study the structure and spatial coherence of this condensate. The $O(N)$ symmetric theory with $N > 1$ is qualitatively different than $N = 1$. We explain the thermodynamical reason why, for $N > 1$, the condensate locally carries nearly maximal conserved charge density. We also show how this property impedes the condensate's decay, and we show that it prevents the condensate from ever becoming fully spatially homogeneous. For $N \leq 4$ the condensate can carry topological defects, but these do not appear to control the large- k tail in its power spectrum, which is the same for $N = 8$ where there are no topological defects.

KEYWORDS: Classical dynamics, scalar field theory, $O(N)$ model, topological defects

Contents

1	Introduction	1
2	General picture	3
3	Describing the Local Condensate	4
3.1	N=1	4
3.2	N greater than 1	5
3.3	Topological considerations	6
4	Effects of Condensate Structure	7
4.1	Local charge density	7
4.2	Ordering dynamics	10
4.3	Condensate decay	14
5	Discussion	16
A	Lattice details	17
B	Oscillation frequencies	18

1 Introduction

Relativistic scalar fields with strongly infrared (IR) initial conditions have been studied for their possible role in post-inflation cosmology [1? ? –3] and as an analogue theory to QCD to study the problem of thermalization immediately after a heavy ion collision. There are physical differences between IR-occupied scalars and nonabelian gauge fields, most notably the role of much more efficient particle-number changing processes in the gauge theory [4], which prevent the formation of infrared condensates [5]. Nevertheless, the theory is of considerable interest for its own merits.

Particularly interesting is the rich infrared physics which is present in a scalar theory when the initial state features large occupancy of relatively IR modes. This problem has been studied extensively for scalar fields with N components, [6–15] using the tools of classical (statistical) field theory, which should be a good approximation in a regime where the occupancy is large. They have found several scaling behaviors in different wave number ranges, some of which have clear explanations in terms of kinetic or 2-particle irreducible descriptions [7]. Here we will study in a little more detail the behavior of the

most infrared modes, well below the effective thermal oscillation frequency induced by mode-mode interactions. Berges *et al* demonstrated three scaling regimes [7, 15]. Below a scale $k_{\text{cond}} \propto t^{-1/2}$ the occupancy is very large and at most weakly k -dependent¹; then it falls steeply, roughly as k^{-5} , until it softens to a $k^{-3/2}$ “energy-cascade” scaling. (Here k is the wave number² and f is a particle occupancy estimate based on the k Fourier component of the field and its time derivative.) We will be interested in these two most-infrared regions. The large occupancy in the deep IR can be understood as a consequence of an approximate particle number conservation. Thermodynamically, the excess particle number in the initial conditions tries to organize into an IR condensate, but by causality it cannot instantly fall into a single $k = 0$ -mode across a large system.

In studying this IR occupancy, we will concentrate on cases with “large” condensates, where the particle number in the deep IR is comparable to the particle number in all other modes, so the IR modes dominate the effective thermal oscillation frequency.³ We will refer to the large occupancy in very IR wave numbers as a “local condensate,” since by local probes it appears to be a condensate and it occurs for the same (particle-number storage) reasons as a true condensate, but it lacks the system-scale long-range order of a true IR condensate, which should reside in one mode. This local condensate then undergoes ordering dynamics, in which it evolves towards higher long-range order. The k -spectrum is a Fourier representation of this ordering dynamics.

We will show that the dynamics of the local condensate depends nontrivially on the number of field components N (we only consider multi-component fields which possess global $O(N)$ symmetry). The case $N = 1$ is qualitatively different than all cases $N \geq 2$. We will explain why, for $N \geq 2$, the condensate locally carries large – nearly maximal – conserved charge density. This phenomenon has previously been observed in the $N = 2$ case [8]. The large local charge density causes the condensate to decay much more slowly for $N > 1$ than for the $N = 1$ case. It also means that, in a finite box, the condensate eventually becomes spatially homogeneous for $N = 1$ but it remains spatially varying for $N \geq 2$, with overall charge neutrality enforcing that the condensate vary in such a way that its total charge is zero. For several N values the ordering dynamics include networks of topological defects, including domain walls for $N = 2$ [8] and strings for $N = 1, 2, 3$ (as we will show). These topological features do not control the high- k tail of the power spectrum, however; this tail is the same when comparing theories with such defects to theories with no defects such as $N = 8$.

¹Ref. [15] find an $f(k) \propto k^{-1/2}$ dependence in the deep infrared. We find k^0 . At this time we do not understand the origin of this discrepancy.

²Since we use a classical framework, we will talk about wave numbers and avoid conflating them with momenta.

³The energy is $\varepsilon \sim \int d^3k \, \omega_k f(k)$; particle number is $n \sim \int d^3k \, f(k)$, and contribution to dispersion corrections is $\sim \int d^3k \, \omega^{-1} f(k)$. If an $\mathcal{O}(1)$ fraction of particles are in the IR, they play a small role in energy but they dominate dispersion corrections.

In the remaining sections we will explain the physics of the results described above, and we will support the description with results from 3+1 dimensional classical (statistical) lattice field theory simulations using $N = 1, 2, 4$, and 8, with lattices of 512^3 and 128^3 points (the former for spectra, the latter to study how the condensate moves into the $k = 0$ and $\vec{k} = \frac{2\pi}{L}[1, 0, 0]$ modes).

2 General picture

Consider $O(N)$ scalar field theory with Lagrangian

$$-\mathcal{L} = \sum_a \left(\frac{1}{2} \partial_\mu \phi_a \partial^\mu \phi_a \right) + \sum_a \frac{m^2}{2} \phi_a^2 + \frac{\lambda}{8} \left(\sum_a \phi_a^2 \right)^2, \quad (2.1)$$

with initial conditions which put a large initial occupancy in IR modes. For suitably large occupancy the fields can be treated as classical. At the lowest order, each k -mode oscillates independently at frequency $\omega_{k,a} = \sqrt{k^2 + \omega_{\text{th},a}^2}$, where the effective thermal oscillation frequency of species a is $\omega_{\text{th},a}^2 \simeq m^2 + \frac{\lambda}{2} \langle 2\phi_a^2 + \sum_b \phi_b^2 \rangle$. At next order, the modes interact with each other, exchanging energy between modes and into formerly unoccupied modes. Entropy considerations tell us that the energy will spread out into all available modes, which for phase-space reasons are dominated by larger- k modes. Scalar theory has an approximately-conserved particle number; for a k -mode with oscillation frequency $\omega_k = \sqrt{k^2 + \omega_{\text{th}}^2}$ and carrying energy $\varepsilon(k)$, the particle number is $f(k) = \varepsilon(k)/\omega_k$. This particle number is not strictly conserved, but it decays on a much longer time scale than the kinetic equilibration needed to re-arrange the energy between k -modes. Now ω_k in UV modes is larger than in the modes occupied in the initial conditions; so as these modes absorb the system's energy, they take little of its particle number, leaving an excess in the IR modes.

Naively, we might expect the modes to take an occupancy of form

$$f(k) \sim \frac{T}{\omega_k - \mu} \quad (2.2)$$

with T and μ the Lagrange multipliers to conserve the system's energy and particle number. For sufficiently large initial n/ε ratio, $\mu = \omega_{\text{th}}$ is not enough to contain all the particle number in the finite- k modes, and an $\mathcal{O}(1)$ fraction of the particle number can go into the mode or modes with the smallest ω_k value, which is permitted by Eq. (2.2) if $\mu = \omega_0$. In practice, Eq. (2.2) can occur at late times if a lattice or other physics provides a UV cutoff, but generally the occupancies take a more complicated form. But the “need” to store a large particle number is a fairly general issue, and a large occupancy in a small k -space region is a general solution.

For statistically uniform initial conditions over a large system, this thermodynamic preference for large occupancy at small k occurs everywhere. Therefore, locally in the

system – on scales large compared to ω_{th}^{-1} but small compared to the system size – particle number should move into a nearly-uniform condensate. But since this occurs due to local physics in a time scale too short for information to be exchanged throughout the system, this condensate will not instantly form coherently – in the same field direction and with the same oscillation phase – everywhere in the system at once. Instead, it will generically form with an independent field direction and oscillation phase at widely spatially separated points. This is similar to a quench process which leads to a vacuum expectation value (VEV), a common phenomenon in condensed matter physics (see for instance [16, 17]) which has also been studied in the context of cosmological phase transitions [18–20].

A uniform true condensate would have a common oscillation phase and field direction throughout the system. This would spontaneously break the symmetry between different oscillation phases and field directions. Therefore the formation of a condensate is a type of symmetry-breaking transition. This is another feature in common with quench processes. But, just as for the formation of a VEV, the local condensate initially chooses its phase and direction independently at widely spaced points. The subsequent dynamics involve the organization of the initially nonuniform features. It is well known that the details of this field organization depend on the space of possible local values (field direction and oscillation phase) for the condensate, which plays the role of the vacuum manifold in the usual case. To simplify the language, we will call the space of possible local values for the condensate the CCspace (condensate configuration space). The topology of this space determines what types of topological structures can occur and impede the ordering dynamics.

Therefore our first order of business is to determine the possible values a condensate can take locally, and to understand the topology of the CCspace.

3 Describing the Local Condensate

The space of field directions and phases which the condensate can take depends in an important way on N the number of field components. For $N = 1$ the theory has no continuous global symmetry, which makes this case essentially different from $N \geq 2$. Therefore we start by considering $N = 1$ and then turn to $N \geq 2$.

3.1 $N=1$

The condensate is described instantaneously by the field value and its time derivative. This is equivalent to the field’s peak amplitude ϕ_0 and the phase of its oscillation, $\phi = \phi_0 \text{Re } e^{i(\varphi + \omega t)}$, where φ is defined modulo 2π . The amplitude is fixed by the particle number density which must enter the condensate, so the variable which can differ through space is the phase φ . Therefore the CCspace has the topology of the circle S^1 .

We also compute the relation between the condensate's peak amplitude ϕ_0 , particle number density n , energy density ε , and oscillation frequency ω , assuming that the condensate's self-interactions dominate its interactions with other fluctuations in establishing the oscillation frequency. Saving the details for Appendix B, we find that

$$\omega = \frac{\sqrt{\pi}\Gamma(3/4)}{\Gamma(1/4)}\sqrt{\lambda}\phi_0 \simeq 0.59907\sqrt{\lambda}\phi_0 \quad (3.1)$$

$$\begin{aligned} &= 1.00751\lambda^{1/4}\varepsilon^{1/4}, \\ \varepsilon &= \frac{3\sqrt{\pi}\Gamma(3/4)}{2^{5/4}\Gamma(1/4)}\lambda^{1/3}n^{4/3} \simeq 0.68825\lambda^{1/3}n^{4/3}. \end{aligned} \quad (3.2)$$

3.2 N greater than 1

Next consider the case of a field with $N \geq 2$ components. The instantaneous value of the condensate is determined by the (locally space-averaged) instantaneous value of ϕ_a and $\dot{\phi}_a$. One possibility is that ϕ_a and $\dot{\phi}_a$ lie in the same field direction. In this case the field oscillates along one field direction as in the $N = 1$ case. The other extreme is for $\dot{\phi}_a$ to be orthogonal in field space to ϕ_a , and of a magnitude which keeps $|\phi|$ unchanged with time. That is, the scalar field can follow a circular orbit through $O(N)$ field space.

The condensate has to carry a certain particle number density. Statistical mechanics arguments favor whichever form for the condensate can do so with minimum energy. Therefore it is important to repeat the calculation of ω , ε , and n as a function of ϕ_0 for the circular orbit case. As shown in Appendix B, for this case we have

$$\omega = \frac{\lambda^{1/2}}{2^{1/2}}\phi_0 = \frac{2^{1/4}}{3^{1/4}}\lambda^{1/4}\varepsilon^{1/4} \simeq 0.9036\lambda^{1/4}\varepsilon^{1/4}, \quad (3.3)$$

$$\varepsilon = \frac{3}{2^{7/3}}\lambda^{1/3}n^{4/3} \simeq 0.5953\lambda^{1/3}n^{4/3}. \quad (3.4)$$

The energy cost of a circular orbit is about 13% lower, at fixed particle number density, than back-and-forth oscillation. Of course, there are also possibilities intermediate between these, corresponding to (precessing) elliptical orbits in field space. These carry energy per particle number strictly intermediate between the two limiting cases we have considered, so the circular-orbit case is the most energetically efficient way to store particle number. Therefore it will be favored on statistical-mechanical grounds.⁴

The circular orbit carries a large local density of at least one of the conserved charges $\rho_{ab} = \dot{\phi}_a\phi_b - \dot{\phi}_b\phi_a$ ($a < b$). One might expect this to forbid circular orbits, since it requires large charge densities and charge is conserved. But charge conservation is global, and the condensate can exchange charge with fluctuations, which propagate freely

⁴Another way to see this is to consider a generic elliptical orbit and to consider the energy cost of adding a quantum in the direction which stretches the ellipse, versus adding a quantum in the direction which makes it more circular. The energy cost is lower for the quantum which makes the oscillation more circular.

into other regions and deposit charge density with the condensate there. Therefore the condensate can take on a large charge density locally, provided that the charge density vary through space such that its space integral vanishes. In the next section we will present numerical evidence showing that this is what occurs.

How do we describe the condensate locally? It is described by the field direction ϕ_a and the field-derivative direction $\dot{\phi}_a$, with the constraints that each is of fixed magnitude (to carry the correct particle number density and maintain minimum energy cost) and that $\dot{\phi}_a$ is orthogonal to ϕ_a . A fixed-length ϕ_a is an element of the $(N-1)$ -sphere S^{N-1} , while a fixed-length orthogonal $\dot{\phi}_a$ is an element of the fixed-length tangent bundle. Therefore the CCspace is topologically the unit-tangent bundle of S^{N-1} , $UT(S^{N-1})$, which is a fibration of S^{N-2} over S^{N-1} .

3.3 Topological considerations

A nontrivial CCspace can have consequences for the ordering dynamics. If the CCspace is not connected – if it has a nontrivial π_0 homotopy group – the condensate in different regions may be separated by domain walls. If it is not simply connected – if the first homotopy group π_1 is nontrivial – it can vary in a topologically nontrivial way around a loop in field space, guaranteeing the existence of string defects. If π_2 is nontrivial, there can be monopole defects. Let us see which occur for some values of N :

1. For $N = 1$ the CCspace is topologically the circle S^1 . This has $\pi_1(S^1) = \mathbb{Z}$ the integers. Therefore there are string defects, corresponding to lines where the condensate's phase changes by 2π as one goes around the line.
2. The case $N = 2$ is equivalent to a complex scalar field. The CCspace is the unit-tangent bundle of the circle S^1 . The unit-tangent space has two points, corresponding to the condensate rotating clockwise or counterclockwise around the complex plane. So the unit-tangent bundle is two copies of the circle, $S^1 \times \mathbb{Z}_2$. Again $\pi_1 = \mathbb{Z}$ and there are strings; but also $\pi_0 = \mathbb{Z}_2$ and there are domain walls, separating regions where the condensate revolves clockwise from regions where it revolves counterclockwise. This is the only N value for which there are domain walls.
3. For $N = 3$ the unit-tangent bundle $UT(S^2)$ is equivalent to $SO(3)$ the group of 3-dimensional rotations. To see why, note that ϕ_a is a direction in \mathcal{R}^3 , while $\dot{\phi}_a$ must be another \mathcal{R}^3 direction orthogonal to the first. Together with their cross product, they define an orthogonal coordinate frame. The space of coordinate frames is the same as the space of rotations (think of the rotation from a standard frame to the desired frame), which is $SO(3)$.

It is important that $SO(3) \neq SU(2)$ its double cover. In particular, since it is double-covered, $\pi_1(SO(3)) = \mathbb{Z}_2$ and there are string defects. However $\pi_0(SO(3))$ and $\pi_2(SO(3))$ are trivial so there are no domain walls or monopoles.

4. For $N = 4$, the tangent bundle of S^3 is trivial, so $UT(S^3) = S^2 \times S^3$. Therefore π_0 and π_1 are trivial, but $\pi_2(UT(S^3)) = \mathbb{Z}$ and there are monopole defects.
5. For general N the unit-tangent bundle is $UT(S^{N-1}) = \text{Spin}(N)/\text{Spin}(N-2)$. For $N > 4$ this space has π_0 , π_1 , and π_2 trivial, so there are no walls, strings, or monopoles. In some dimensions π_3 is nontrivial and there are textures, but for the special case $N = 8$, $UT(S^7) = S^6 \times S^7$, which has no homotopy below π_6 and so is free of defects in 3+1 dimensional space.⁵

4 Effects of Condensate Structure

Here we will look at the consequences of the form of the condensate, and check them against numerical investigations.

4.1 Local charge density

The most convincing evidence that the above description of condensation is true is to look at the process in a small enough volume that it reaches completion. Then we analyze the late-time behavior and see that it is qualitatively different for the cases $N = 1$, $N = 2$, and $N > 2$.

For $N = 1$ there is no obstacle to the condensate developing completely in the $k = 0$ mode. But for $N > 1$ the condensate locally carries a net abundance of conserved charge, which should average to zero globally. Therefore the condensate should *not* become completely uniform, but should always vary in such a way that the global charge vanishes. For $N = 2$ this requires a pair of domain walls, separating the regions with positive and negative charge density. Such domain walls were observed and characterized in [8]. For $N > 2$ there are several charges, and the charge density can revolve smoothly through the $N(N-1)/2$ dimensional space of possibilities.

First we look for this behavior in Fourier space, by evolving $N = 1, 2, 3$ systems in 128^3 boxes, which allows us to achieve times where the condensate completes its evolution towards the infrared. Fig. 1 shows the total power in the $k = \frac{2\pi}{L}(0, 0, 0)$ mode, and the sum of power in $k = \frac{2\pi}{L}(\pm l, 0, 0)$, $\frac{2\pi}{L}(0, \pm l, 0)$ and $\frac{2\pi}{L}(0, 0, \pm l)$ for $l = 1, 2, 3$, for a typical simulation. That is, it shows the total power in each of the four lowest Fourier modes for which k lies purely along a lattice direction. For the case $N = 1$ we see that the power all moves into the $k = 0$ mode, which then decays with time. For $N = 3$ the power is shared equally between the $k = 0$ mode and the modes of form $k = (\pm 1, 0, 0)\frac{2\pi}{L}$.

⁵I thank Johannes Walcher for a refresher on unit tangent bundles.

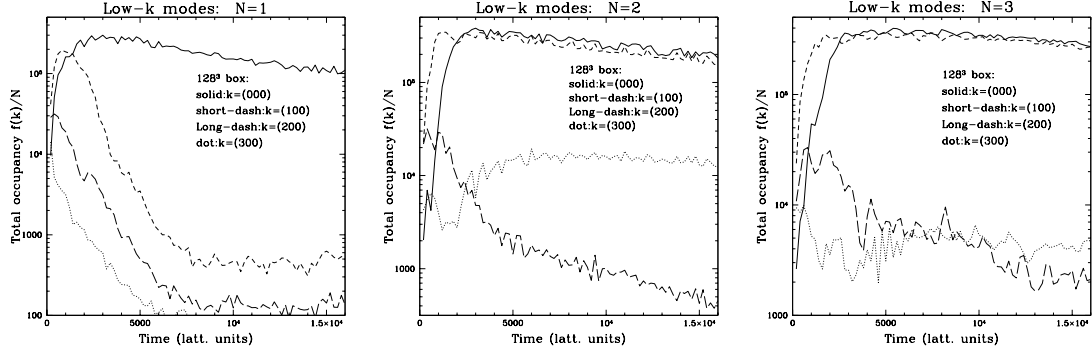


Figure 1. Power in the lowest k -modes which point along a lattice direction, for $N = 1, 2, 3$ (left to right). For $N = 1$ the power all concentrates into the lowest mode. For the other cases, the power is shared equally between the $k = 0$ mode and the next-lowest mode; for $N = 2$ there is also power in the $k = (3, 0, 0)$ mode.

It is also shared equally between ϕ^2 and $\dot{\phi}^2$, in that the ratio $\langle \dot{\phi}^2 \rangle / \langle \phi^2 \rangle$ summed over the lowest modes remains fixed, rather than oscillating as it does for $N = 1$. The case $N = 2$ is superficially similar to the $N = 3$ case, except that the power in $l = 3$ does not decay but remains much larger than the power in $l = 2$ (or any of the other Fourier modes, such as $k = \frac{2\pi}{L}(1, 1, 0)$, which are not along lattice directions). This is because, for $N = 2$, the condensate is discontinuous across a domain wall, which leaves power in all odd harmonics, while for $N = 3$ the charge density is smooth. We also studied $N = 4$, which shows the same behavior as $N = 3$.

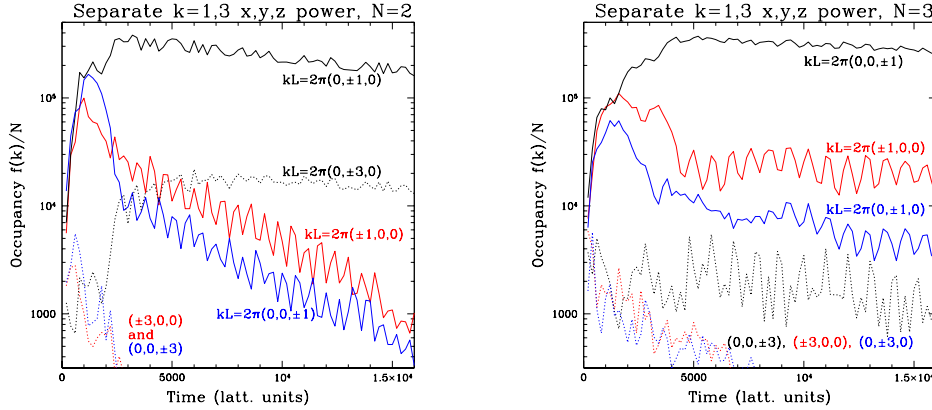


Figure 2. Power in the lowest nonzero Fourier mode along the x , the y , and the z axis, as well as the $(3, 0, 0)$ -type modes. Left: $N = 2$. Right: $N = 3$. In each case, the power along two axes dies away, while the third axis persists. For $N = 2$ it is the same axis where there is persistent power in the $(0, 3, 0)$ modes.

What Fig. 1 does not show is that the power in $(1,0,0)$ type modes is in fact all concentrated in the mode along one axis. To see this, in Fig. 2 we plot separately the power in $k = \frac{2\pi}{L}(\pm 1, 0, 0)$ and that in $k = \frac{2\pi}{L}(0, \pm 1, 0)$ and $(0, 0, \pm 1)$, for $N = 2$ and $N = 3$. We also plot the $(3,0,0)$ power, to see that it is supported along the same lattice direction as the $(1,0,0)$ power for the $N = 2$ case where it does not die off. The fact that the power ended up along one axis indicates that the condensate remains spatially asymmetric in this, but not the other two, lattice directions. We performed each simulation several times with different random number seeds, and found that the lattice axis where the breaking occurs is randomly different, but the pattern shown above is the same for each simulation; for $N > 1$ the power equipartitions between the $(0,0,0)$ mode and one set of $(\pm 1, 0, 0)$ modes and is small in the others.

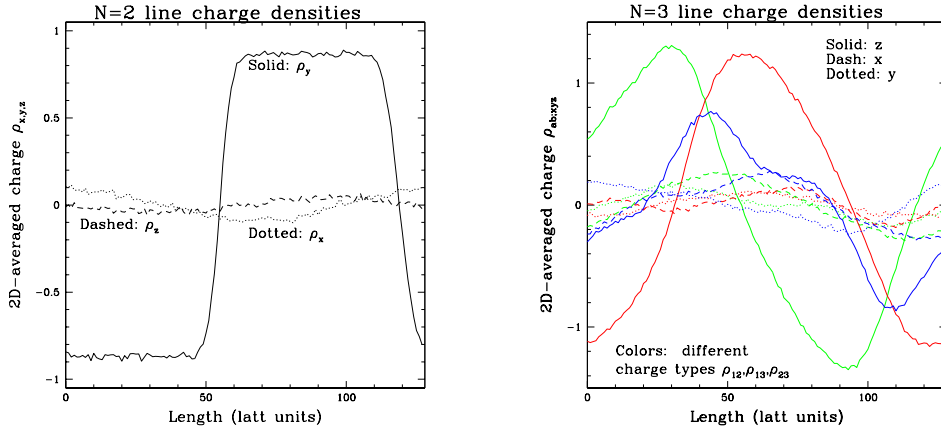


Figure 3. plane-averaged charge density plotted along the remaining axis, in 128^3 box at $t = 10,000$ when the condensate has settled into its final form. Left: $N = 2$ case, where the charge density varies along the y axis. Right: $N = 3$ case, where the three charge densities vary primarily in the z direction.

To see it another way, let us define the charge density averaged over two lattice directions as a function of the third: $\rho_{ab;x} \equiv L^{-2} \int dy dz \rho_{ab}(x, y, z)$ and similarly for $\rho_{ab;y}$ and $\rho_{ab;z}$. We plot this, for each axis and at a fixed late time $t = 10,000$ lattice units, in Fig. 3. On the left, we see that the $N = 2$ theory has a pair of sharp discontinuities in ρ_y , with plateaux between. For $N = 3$ we see that each charge component varies smoothly such that $\sum_{ab} \rho_{ab;z}^2$ is nearly constant and much larger than in the other two directions. Note that these measurements were made directly on the fields without any smearing and no averaging except for the averaging over lattice planes. Averaging over 2D planes is already enough to suppress the contribution from UV modes, without any field smearing.

We can also form a histogram of the value of ρ at each point on the lattice. The result

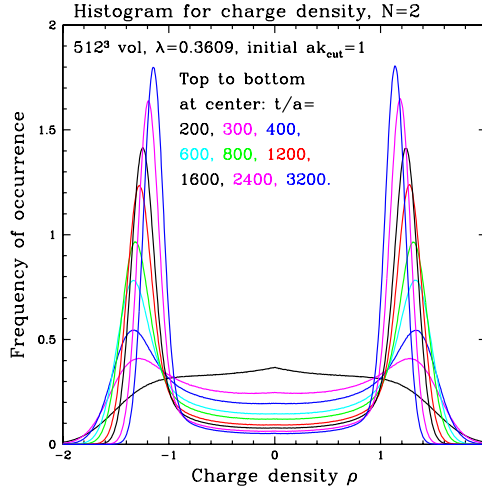


Figure 4. Histogram of the condensate’s local charge density, for the $N = 2$ theory in a 512^3 box after smearing ϕ and $\dot{\phi}$ to eliminate the contribution of UV fluctuations.

looks fairly Gaussian, because of the large site-by-site contribution from UV fluctuations. But if we first smooth the fields, the result is different. Sticking with the $N = 2$ theory, we Fourier transformed ϕ and $\dot{\phi}$, multiplied by $\phi(k) \rightarrow \phi(k) \exp(-k^2/\omega^2)$, $\dot{\phi}(k) \rightarrow \dot{\phi}(k) \exp(-k^2/\omega^2)$ (with ω determined from the data as described in Appendix A), and Fourier transformed back, in order to eliminate the contribution of UV fluctuations. Then we determined the charge density due to IR fields at each lattice point by finding $\rho(x) = i(\phi^* \dot{\phi}(x) - \dot{\phi} \phi^*(x))$ as usual. Fig. 4 shows a histogram of how common each possible value of the charge density is, for several times and in a 512^3 box. The curves are normalized so the area under each curve is 1. At late times there are two sharp peaks with a plateau in between; we interpret the peaks as arising from points within regions of one or the other charge phase, and the plateau as the contribution from the domain walls separating these phases.

4.2 Ordering dynamics

Next consider a large lattice volume 512^3 and somewhat shorter times, which allows us to see the field organization dynamics of the local condensate. As we have emphasized, for $N \leq 4$ the condensate can carry topological defects. A topological defect is a location where the condensate field varies abruptly. Therefore it is guaranteed to create power-law tails in the high- k part of the power spectrum for the condensate. Specifically, a network of domain walls should create k^{-4} tails in the power spectrum; strings should create k^{-5} tails, and monopoles should create k^{-6} tails.⁶ To illustrate this behavior,

⁶In general the power is k^{-d-c} with d the space dimension and c the codimension of the defect. Consider a defect with codimension c and dimension $d-c$. A function in c dimensions which is discontinuous

consider Eq. (2.1) with $m^2 < 0$ and adding a damping term to the dynamics such that

$$\text{Dissipative dynamics: } \partial_t^2 \phi_a = -\tau \partial_t \phi_a + \nabla^2 \phi_a + V_{,\phi_a}. \quad (4.1)$$

In our numerical implementation we chose $\tau = a/2$ so the damping dynamics are strong, and we chose $a^2 m^2 = -0.5$ and $\lambda = 1$ so the VEV is $|\phi| = 1$ in lattice units and the radial fluctuations have oscillation frequency $1/a$. In this case the field forms a true condensate, but we choose random initial conditions, so the field starts out disordered and must follow ordering dynamics. The ordering dynamics are impeded by topological defects with codimension N : walls for $N = 1$, strings for $N = 2$, monopoles for $N = 3$, textures for $N = 4$, but no topological structures for $N = 5$. By the arguments above, we expect the power spectrum for $N = 1, 2, 3$ to display $k^{-(3+N)}$ tails, and indeed it does. Fig. 5 shows the power spectrum at several times for the case $N = 2$, first with fixed axes and then with axes rescaled such that the curves collapse onto a single scaling behavior. Finally, the scaling behavior is compared for $N = 1, 2, 3, 5$ (at time $t = 960a$). The IR behavior after scaling to k_{cond} looks similar for all cases, but the larger- k behavior is different. For $N = 1, 2, 3$ we see power laws with k^{-3-N} power, and for $N = 5$ the tail does not asymptote to a power, all as expected. Note that for $N = 1, 2$ the spectrum is actually steeper than k^{-3-N} around $k = 1.8k_{\text{cond}}$, before taking the power-law form at $k > 2k_{\text{cond}}$.

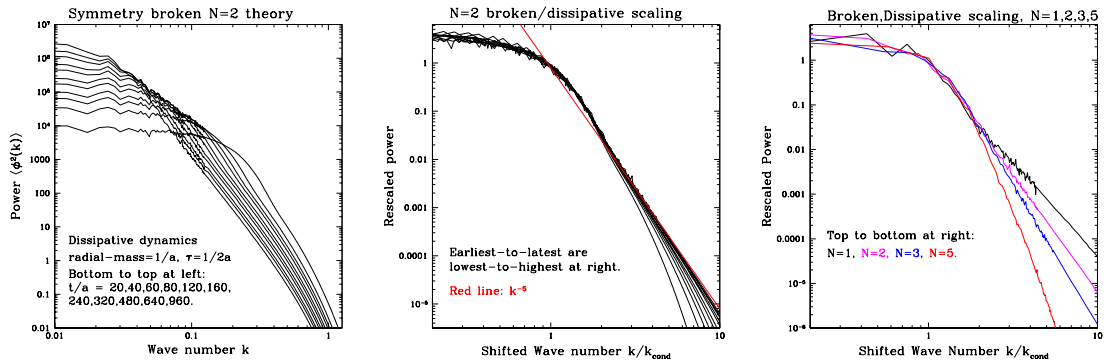


Figure 5. Power spectrum for broken-symmetry theory under dissipative dynamics, to illustrate the effect of defects on the spectrum. Left: $N = 2$ theory at several times. Middle: rescaling $k \rightarrow k/k_{\text{cond}}$ and power by $2\pi^2 k_{\text{cond}}^{-3}$ so the curves collapse onto a scaling form. Right: scaling form for $N = 1, 2, 3, 5$ superposed, showing different power-law tails.

We also see in the two left plots of Fig. 5 that the power-law tails break off at a larger- k scale which stays fixed in physical units. This scale is set by the thickness of the defects; at this scale the spatial features become smooth so the power spectrum changes at a point has a Fourier spectrum with k^{-2c} tails; but each of the remaining $d - c$ dimensions “along” the defect dilute this by an additional power.

from power to exponential behavior. Again we emphasize that this discussion is only to show the effect of defects on the power-law tails.

Returning to the theory with a particle-number condensate, we expect the topological structures to be *one* contribution to the IR tail of the condensate's part of the power spectrum. There can also be ordinary nontopological fluctuations in the condensate, which will obscure the topological contribution if they have a softer power law or substantially larger amplitude. We also expect the defect core size to depend on N , now differing between the $N = 2$ case and other cases. For string or monopole defects we expect the core size to be $\sim \omega^{-1}$. But for domain walls, we argue that it should be at least 3 times larger. Generally the thickness of a domain wall is set by the potential energy cost of the state at the center of the wall, with inverse width $k_{\text{wall}} \propto \sqrt{V}$. The core of the domain wall contains condensate which is not locally charged but oscillates straight back-and-forth. The excess energy cost of this state is only about 13% of the condensate's energy density, so we expect the wall's inverse thickness to have an extra power of $\sqrt{0.13}$.

Fig. 6 shows the analogous figures to Fig. 5, but for the theory with a condensate. The time-dependence of the spectra in the infrared is superficially similar to that in Fig. 5. As expected, this behavior flattens out at larger k rather than getting steeper. In the $N = 1$ case, but not for any other N , there is also a feature around $ak = 0.9$. This peak is the freshly-produced excitations of frequency $2\omega_0$, generated from the decay of the condensate, see [14] and the next subsection.

Fig. 6 also shows the spectra rescaled to have the same total power and characteristic wave-number k_{cond} . It shows excellent collapse onto a scaling solution, broken at a larger- k scale which grows, in units of k_{cond} , as time progresses.⁷ This collapse onto a scaling function has already been observed by previous authors [7, 15]. In [7] it is argued that the steep part of the spectrum below k_{cond} should behave as $f \propto k^{-5}$. We find $k^{-4.5}$, which is the slope of the straight line in the lower-left frame of the figure, which agrees with the numerical results in [15]. A k^{-5} line visibly fails to fit (not shown).

Finally, in the lower right we show the scaling solutions for $N = 1, 2, 3, 4, 8$ all superposed. Beyond about $k = 7k_{\text{cond}}$ the curves deviate from scaling, so this behavior should be ignored. The curves agree strikingly well, in strong contrast to the symmetry-broken case of Fig. 5. This collapse of different times and N values onto a single scaling solution has previously been pointed out by [7, 15]. These authors argued that the concordance indicates a universality in the physical origin of the spectrum. This is rather surprising, given the differences in condensate structure and topological obstructions which we have previously discussed. Therefore it does *not* appear that topological structures control the tail's behavior, at least for the cases other than $N = 2$.

It is a little puzzling that a k^{-4} tail does not emerge for the $N = 2$ case, since we

⁷The physical scale decreases, as we see in the upper plots; but k_{cond} decreases faster.

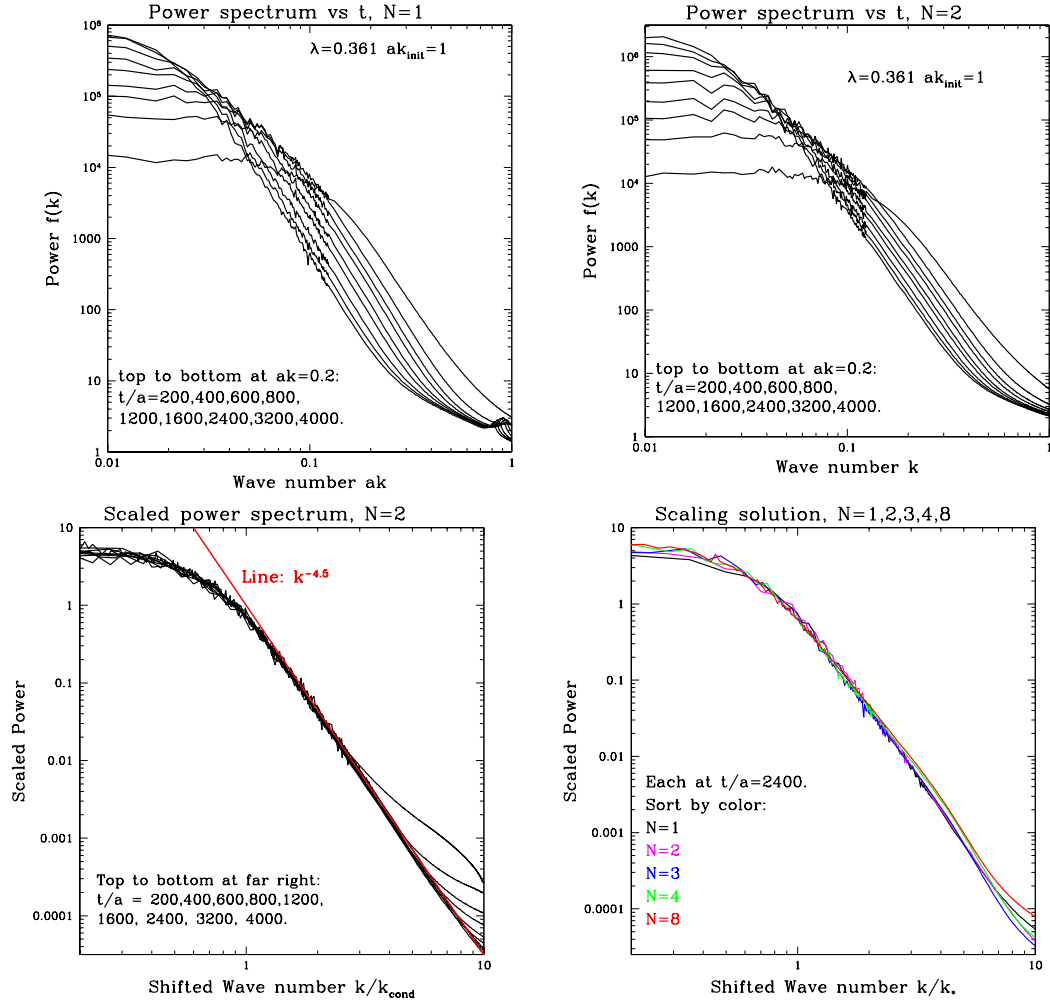


Figure 6. Power spectrum of the IR condensate. Top: power spectrum at several times for $N = 1$ theory (left) and $N = 2$ theory (right). Bottom left: rescaled version for $N = 2$ showing scaling behavior. Bottom right: scaled spectrum at $t = 2400$ for $N = 1, 2, 3, 4, 8$.

have already seen that there are domain walls in the charge-sign of the condensate. One possibility is that a k^{-4} region would emerge if we could achieve a much wider scaling window. After all, for the symmetry-breaking theory in Fig. 5, the scaling emerges relatively late, and as discussed above we expect it to break down by $k \sim \omega/3$ because the walls are quite thick. Unfortunately, achieving a significantly wider scaling window is prohibitively numerically costly.

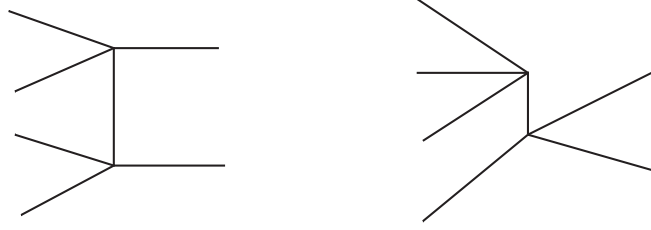


Figure 7. Feynman diagrams for $4 \rightarrow 2$ number-changing scattering.

4.3 Condensate decay

The presence of a large local charge density has consequences for how the condensate decays with time. To see this, consider the Feynman diagrams responsible for condensate decay; $4 \rightarrow 2$ scattering as shown in Fig. 7. For the $N = 1$ theory, the leading cause of condensate decay is the case where the 4 incoming particles are drawn from the condensate and the two outgoing particles are finite- k excitations, each carrying 2ω energy. The two diagrams partially cancel, since one has a spacelike propagator and one has a timelike propagator above the mass shell.

It is actually not straightforward to compute the diagram, since the dispersion relation for the outgoing particles and virtual propagators are not simply those of a massive particle – the coherence of the condensate is not the same as $\langle \phi^2 \rangle$ arising from many independent fluctuations. But we can parametrically estimate the rate fairly easily. Though the calculation can be done within the classical theory, we will use the notation of the quantum theory because it is probably more familiar to our readers. The rate of particle number change from the condensate is determined by the Boltzmann equation for the condensate particles:

$$\begin{aligned}
\frac{dn_{\text{cond}}}{dt} &\sim \int \frac{d^3 p_{1,2,3,4} d^3 k_{1,2}}{p_1 p_2 p_3 p_4 k_1 k_2} |\mathcal{M}|^2 \delta^4 \left(\sum p_i - \sum k_i \right) \\
&\quad \times (f_{p_1} f_{p_2} f_{p_3} f_{p_4} [1 + f_{k_1}] [1 + f_{k_2}] - [1 + f_{p_1}] [1 + f_{p_2}] [1 + f_{p_3}] [1 + f_{p_4}] f_{k_1} f_{k_2}) \\
&\sim \int \frac{d^3 p_{1,2,3,4}}{p_1 p_2 p_3 p_4} f_{p_1} f_{p_2} f_{p_3} f_{p_4} \frac{d^3 k_{1,2}}{k_1 k_2} (f_{k_1} + f_{k_2}) |\mathcal{M}|^2 \delta^4 \left(\sum p_i - \sum k_i \right) \\
&\sim \lambda^4 \frac{n_{\text{cond}}^4}{\omega^8} f(2\omega).
\end{aligned} \tag{4.2}$$

Here $n_{\text{cond}} = \int d^3 p f(p)$ is the particle number density in the condensate, λ^4 arises from the squared matrix element, and the powers of ω enter on dimensional grounds from the remaining phase space integrals and the matrix element.

Naively this result seems to state that the condensate's decay rate is a very steep power of the condensate's size n_{cond} . But the presence of ω^{-8} in the final expression moderates this, because the dominant contribution to the oscillation frequency is actually

the condensate itself. Indeed, if we ignore the contribution from all other fluctuations, we have, from Eq. (B.4) and Eq. (B.6),

$$\omega \sim \lambda^{1/4} \varepsilon^{1/4} \quad \text{and} \quad \varepsilon \sim \lambda^{1/3} n_{\text{cond}}^{4/3} \quad \Rightarrow \quad \omega^3 \sim \lambda n_{\text{cond}}. \quad (4.3)$$

Therefore we expect weaker n_{cond} dependence: $dn_{\text{cond}}/dt \propto n_{\text{cond}}^{4/3} f(2\omega)$. If, for instance, $f(2\omega) \propto \omega^{-3/2}$, this would give $dn_{\text{cond}}/dt \propto n_{\text{cond}}^{5/6}$. In general $f(2\omega)$ also varies (decreases) with time. And any other contribution to the oscillation frequency, such as an explicit m^2 term or a contribution from other excitations, can also substantially slow the condensate's decay, especially once n_{cond} has already gotten smaller.

We actually see the consequences of this decay process in Fig. 6. In the upper left panel, the power spectrum has a bump around $ak = 0.9$ which moves to lower k at late time as ω shrinks (since $\omega \propto n_{\text{cond}}^{1/3}$). These are the condensate decay products which have not yet rescattered into other wave numbers – as already realized in [14]. The same peak does not occur for $N = 2$, as the figure shows and for reasons we will now see.

The situation is quite different for $N \geq 2$ because the condensate is maximally charged. The process in Fig. 7 cannot occur if all 4 initial particles are from the condensate, because all incoming particles have the same $O(N)$ charge, so the process violates charge conservation and the relevant diagrams vanish identically. Instead, 3 condensate particles must pick up one particle of opposite charge from the thermal bath to produce two final-state particles with the same charge as the condensate. These are then free to propagate to a different region to keep the fluctuations locally charge-neutral. In Eq. (4.2), one of the $\int d^3p f_p$ must return the number of normal excitations, $n_{\text{cond}} \rightarrow \omega^3 f(\sim 1\omega)$. The decay rate of the condensate is estimated as

$$\frac{dn_{\text{cond}}}{dt} \sim \lambda^4 \frac{n_{\text{cond}}^3}{\omega^5} f^2(\sim 1\omega) \quad (4.4)$$

which is smaller than the previous estimate by a factor of $\sim \omega^3 f(\sim 1\omega)/n_{\text{cond}}$, which is the ratio of infrared but non-condensate excitations to condensate excitations. The condensate should decay much more slowly for $N \geq 2$ than for $N = 1$, especially in the regime where the condensate is large. It also does not decay into particles of a specific k value, since there is an energy and momentum range for the particle picked up from the medium – hence the absence of a peak around $k \sim \sqrt{3}\omega$ in the upper-right plot in Fig. 6.

We explore condensate decay as a function of N in Fig. 8, which shows the particle number in the condensate (total particle number at small k as defined in Appendix A) as a function of time for the $N = 1, 2, 3, 4, 8$ theories. The figure shows a stark difference between the $N = 1$ case, where there is no charge-conservation constraint, and the $N > 1$ cases, where there is. Note that the initial particle number, and the particle number which needs to move into the condensate, scales as N for our initial conditions;

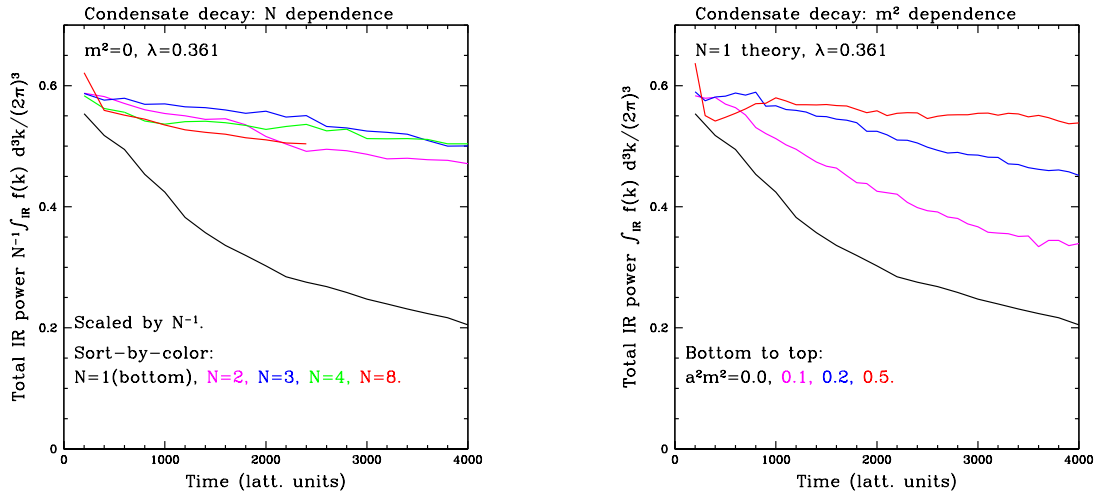


Figure 8. Condensate as a function of time for the $N = 1, 2, 3, 4, 8$ theories, left; condensate as a function of time as the explicit m^2 term is increased for the case $N = 1$, right.

we have explicitly removed this factor in the figure. We also study the effect of including an explicit m^2 term, which raises the oscillation frequency and therefore suppresses the condensate decay according to Eq. (4.2), for the $N = 1$ case. For the parameters studied, the $m^2 = 0$ case has $a^2\omega^2 \sim 0.3$, so the first two $m^2 > 0$ curves still have the oscillation frequency dominated by the condensate’s self-interactions; nevertheless, the addition of an explicit m^2 term raises ω^2 enough to substantially suppress the condensate’s decay. We have not yet tried to explain these curves quantitatively, though it would be interesting to do so in future. They certainly support qualitatively the expectations explained above.

5 Discussion

We have considered the deep IR behavior of classical scalar field theory, where the approximate conservation of particle number causes the development of a particle-number storing condensate. Because condensate formation occurs locally throughout the system, the condensate is initially incoherent, and must develop long-range order. Our most interesting result is that, in the case that the condensate is large enough that its self-interactions dominate its oscillation frequency, the condensate’s local structure is qualitatively different in single-component ($N = 1$) theory than in $O(N)$ symmetric $N \geq 2$ component theories. In the latter case, the condensate locally carries the maximal possible charge density, with overall charge neutrality maintained by spatial inhomogeneity of the condensate. This inhomogeneity persists indefinitely in finite volume, and the charge density impedes the decay of the condensate, which is much slower

for $N > 1$ than for $N = 1$. Finally, we have considered the large- k tail of the condensate, which appears to fall as a power law which is *not* determined by the topological structures present due to the long-range disorder of the condensate.

Acknowledgments

I would like to thank Thomas Epelbaum and Jürgen Berges for helpful conversations, Johannes Walcher for help on homotopy for some specific spaces, and Paul Mercure for his patience.

A Lattice details

We give a few details of our lattice implementation. We discretize the theory of Eq. (2.1) on the lattice with a standard nearest-neighbor implementation of the gradient term and leapfrog update rule, with temporal step equal to 1/10 of the spacing. Our initial conditions are $\phi_a = 0$ and each k -mode $\dot{\phi}_a(k)$ drawn from a Gaussian distribution of fixed width for $k < k_{\text{init}}$ (technically, $\tilde{k}^2 \equiv \sum_{i=1,2,3} 2 - 2\cos(k_i a) < k_{\text{init}}^2$) and zero for $k > k_{\text{init}}$. In practice we use $k_{\text{init}} = 1/a$, a the lattice spacing. This provides large occupancy per unit energy, so that as the energy fills into all available modes and in particular into higher- k modes, there is excess particle number which must fill the IR condensate. We choose $m^2 = 0$ except in a few simulations where we study its effect on the condensate's time evolution.

The field normalization and λ value overdefine the system; one is free to rescale $\phi \rightarrow \xi\phi$, with ξ a constant, simultaneously rescaling $\lambda \rightarrow \xi^{-2}\lambda$. We normalize the field so the total energy is N per lattice site. We chose this convention because, to the extent that the system is weakly coupled, the eventual equilibrium (after the condensate decays) has energy equipartitioned between kinetic and potential+gradient energy, and this corresponds to an energy of $\frac{1}{2}$ per degree of freedom, and hence to a temperature of 1. With this convention, our simulations all used $\lambda = 0.361$. This value kept the thermal oscillation frequency somewhat below $a\omega_{\text{th}} = 1$ so that the IR behavior should not be too contaminated by lattice effects but the dynamic range is still relatively good.

When we Fourier transform the ϕ and $\dot{\phi}$ fields to form a power spectrum, we treat $k^2 < 8/aL$ separately from $k^2 > 8/aL$ (where a is the lattice spacing and L is the box length). For the former, we bin all Fourier components with the same value of k^2 , eg, $k = \frac{2\pi}{L}(2, 2, 1)$ is combined with its cubic-invariance equivalents and with $k = \frac{2\pi}{L}(3, 0, 0)$ but not with $(3, 1, 0)$. For $k^2 > 8/aL$ we use \tilde{k}^2 bins of width $2/aL$.

We define a range of wave numbers as being the range which contains the condensate by finding the bin with the largest average Fourier power in $\omega^2\langle\phi^2(k)\rangle + \langle\dot{\phi}^2(k)\rangle$, and considering all bins where this quantity is at least 1/300 of this maximum value. We

then find the integral of $\langle \phi^2(k) \rangle$ and $\langle \dot{\phi}^2 \rangle$ over this range, and find ω^2 self-consistently as

$$\omega^2 = \frac{\sum_{\text{cond.modes}} \dot{\phi}^2(k)}{\sum_{\text{cond.modes}} \phi^2(k)}, \quad (\text{A.1})$$

re-determining the range of modes in the condensate until we reach self-consistency. The occupancy at k is estimated as

$$f(k) = \omega \langle \phi^2(k) \rangle + \omega^{-1} \langle \dot{\phi}^2(k) \rangle. \quad (\text{A.2})$$

These steps assume that the condensate is carried in a range of k such that $k^2 \ll \omega^2$, which becomes true quite quickly; if it is not true it does not make sense to speak of a local condensate. Finally, we define the characteristic wave-vector for the local condensate as

$$k_{\text{cond}} = \frac{\sum_{\text{cond.modes}} k f(k)}{\sum_{\text{cond.modes}} f(k)}. \quad (\text{A.3})$$

B Oscillation frequencies

Here we complete the details in the calculation of oscillation frequencies for single-component and “circular” multi-component oscillation.

Consider a scalar oscillating back-and-forth in a $(\lambda/8)\phi^4$ potential. If the field oscillates with amplitude ϕ_0 then the energy is

$$\varepsilon = \frac{\lambda}{8}\phi_0^4 = \frac{1}{2}\dot{\phi}^2 + \frac{\lambda}{8}\phi^4 \quad \rightarrow \quad \dot{\phi} = \frac{\sqrt{\lambda}}{2}\sqrt{\phi_0^4 - \phi^4} \quad (\text{B.1})$$

and the period of the oscillation is

$$\begin{aligned} \frac{T}{4} &= \int_0^{\phi_0} \frac{dt}{d\phi} d\phi = \int_0^{\phi_0} \frac{1}{\sqrt{2\varepsilon - 2V(\phi)}} d\phi = \frac{2}{\phi_0 \sqrt{\lambda}} \int_0^1 \frac{dx}{\sqrt{1 - x^4}} \\ &= \frac{\sqrt{\pi}\Gamma(1/4)}{2\Gamma(3/4)\phi_0 \sqrt{\lambda}} \end{aligned} \quad (\text{B.2})$$

which gives a frequency of⁸

$$\omega = \frac{2\pi}{T} = \frac{\sqrt{\pi}\Gamma(3/4)}{\Gamma(1/4)} \sqrt{\lambda} \phi_0 \simeq 0.59907 \sqrt{\lambda} \phi_0. \quad (\text{B.3})$$

⁸This is not the same as the naive estimate $\omega^2 = \frac{3\lambda}{2} \langle \phi^2 \rangle$, with

$$\langle \phi^2 \rangle = \frac{\int_0^{\phi_0} d\phi \frac{\phi^2}{d\phi/dt}}{\int_0^{\phi_0} d\phi \frac{1}{d\phi/dt}} = \frac{\phi_0^2 \int_0^1 dx x^2 / \sqrt{1 - x^4}}{\int_0^1 dx / \sqrt{1 - x^4}} = \phi_0^2 \frac{\Gamma^2(3/4)}{\Gamma(5/4)\Gamma(1/4)}$$

which gives $\omega = .8279 \sqrt{\lambda} \phi_0$. This estimate may work for larger- k excitations, but it does not work at $k = 0$ because the field is time-coherent with itself.

We can re-cast this in terms of the energy density using $\varepsilon = \lambda\phi_0^4/8$:

$$\omega = \frac{(8\pi^2)^{1/4}\Gamma(3/4)}{\Gamma(1/4)}\lambda^{1/4}\varepsilon^{1/4} = 1.00751\lambda^{1/4}\varepsilon^{1/4}. \quad (\text{B.4})$$

When we add one particle to the condensate, we add an energy of ω . So the particle number stored in the condensate is⁹

$$n(\varepsilon) = \int_0^\varepsilon \frac{d\varepsilon'}{\omega} = \frac{4}{3} \frac{\varepsilon}{\omega} = \frac{4}{3(1.00751)\lambda^{1/4}}\varepsilon^{3/4}. \quad (\text{B.5})$$

Alternatively,

$$\varepsilon \simeq 0.68825\lambda^{1/3}n^{4/3}. \quad (\text{B.6})$$

Now consider instead a scalar in 2 or more components, with $\dot{\phi}$ orthogonal to ϕ and large enough that the field's amplitude remains fixed at ϕ_0 while changing direction in field space. This is like circular orbital motion in an r^4 potential. The energy density is

$$\varepsilon = \frac{1}{2}\dot{\phi}_0^2 + \frac{\lambda}{8}\phi_0^4 \quad (\text{B.7})$$

and the Virial relation $\frac{1}{2}\dot{\phi}^2 = 2\frac{\lambda}{8}\phi_0^4$ gives

$$\varepsilon = \frac{3}{4}\dot{\phi}_0^2 = \frac{3\omega^2}{4}\phi_0^2 = \frac{3\lambda}{8}\phi_0^4 \quad \text{and} \quad \omega^2 = \frac{\lambda}{2}\phi_0^2 \quad (\text{B.8})$$

from which we easily find

$$\omega = \frac{2^{1/4}}{3^{1/4}}\lambda^{1/4}\varepsilon^{1/4} \simeq 0.9036\lambda^{1/4}\varepsilon^{1/4}. \quad (\text{B.9})$$

Following the same steps as before, we find

$$n(\varepsilon) = \frac{4\varepsilon}{3\omega} = \frac{2^{7/4}}{3^{3/4}\lambda^{1/4}}\varepsilon^{3/4} \quad (\text{B.10})$$

which equals $n = \phi_0\dot{\phi}_0 = \omega\phi_0^2$ as expected, and

$$\varepsilon \simeq \frac{3}{2^{7/3}}\lambda^{1/3}n^{4/3} \simeq .59528\lambda^{1/3}n^{4/3}. \quad (\text{B.11})$$

Therefore the energy associated with a condensate which makes a circular rotation in field space is lower, at fixed number density, than the energy for the condensate to oscillate straight back-and-forth.

⁹If this looks strange, recall the behavior of a quantum system with potential V in the WKB approximation, valid for high levels. The level number f is given in terms of the level energy E by $f = \frac{1}{\pi} \int_{\phi|V(\phi) < E} \sqrt{2(E - V)} d\phi$. The level spacing dE/df sets the oscillation frequency of a superposition of levels, So the period is given by $T = 2\pi/\omega = 2\pi df/dE$ which is $T = 4 \int (2(E - V))^{-1} d\phi$, agreeing with Eq. (B.2).

References

- [1] L. Kofman, A. D. Linde, and A. A. Starobinsky, *Reheating after inflation*, *Phys. Rev. Lett.* **73** (1994) 3195–3198, [[hep-th/9405187](#)].
- [2] S. Yu. Khlebnikov and I. I. Tkachev, *Classical decay of inflaton*, *Phys. Rev. Lett.* **77** (1996) 219–222, [[hep-ph/9603378](#)].
- [3] T. Prokopec and T. G. Roos, *Lattice study of classical inflaton decay*, *Phys. Rev.* **D55** (1997) 3768–3775, [[hep-ph/9610400](#)].
- [4] P. B. Arnold, G. D. Moore, and L. G. Yaffe, *Effective kinetic theory for high temperature gauge theories*, *JHEP* **01** (2003) 030, [[hep-ph/0209353](#)].
- [5] A. Kurkela and G. D. Moore, *UV Cascade in Classical Yang-Mills Theory*, *Phys. Rev.* **D86** (2012) 056008, [[arXiv:1207.1663](#)].
- [6] J. Berges, A. Rothkopf, and J. Schmidt, *Non-thermal fixed points: Effective weak-coupling for strongly correlated systems far from equilibrium*, *Phys. Rev. Lett.* **101** (2008) 041603, [[arXiv:0803.0131](#)].
- [7] J. Berges and D. Sexty, *Strong versus weak wave-turbulence in relativistic field theory*, *Phys. Rev.* **D83** (2011) 085004, [[arXiv:1012.5944](#)].
- [8] T. Gasenzer, B. Nowak, and D. Sexty, *Charge separation in Reheating after Cosmological Inflation*, *Phys. Lett.* **B710** (2012) 500–503, [[arXiv:1108.0541](#)].
- [9] J. Berges and D. Sexty, *Bose condensation far from equilibrium*, *Phys. Rev. Lett.* **108** (2012) 161601, [[arXiv:1201.0687](#)].
- [10] M. Schmidt, S. Erne, B. Nowak, D. Sexty, and T. Gasenzer, *Nonthermal fixed points and solitons in a one-dimensional Bose gas*, *New J. Phys.* **14** (2012) 075005, [[arXiv:1203.3651](#)].
- [11] J. Berges, S. Schlichting, and D. Sexty, *Over-populated gauge fields on the lattice*, *Phys. Rev.* **D86** (2012) 074006, [[arXiv:1203.4646](#)].
- [12] B. Nowak, S. Erne, M. Karl, J. Schole, D. Sexty, and T. Gasenzer, *Non-thermal fixed points: universality, topology, & turbulence in Bose gases*, 2013. [[arXiv:1302.1448](#)].
- [13] M. Karl, B. Nowak, and T. Gasenzer, *Universal scaling at nonthermal fixed points of a two-component Bose gas*, *Phys. Rev.* **A88** (2013), no. 6 063615, [[arXiv:1307.7368](#)].
- [14] J. Berges, K. Boguslavski, S. Schlichting, and R. Venugopalan, *Basin of attraction for turbulent thermalization and the range of validity of classical-statistical simulations*, *JHEP* **05** (2014) 054, [[arXiv:1312.5216](#)].
- [15] A. P. Orioli, K. Boguslavski, and J. Berges, *Universal self-similar dynamics of relativistic and nonrelativistic field theories near nonthermal fixed points*, *Phys. Rev.* **D92** (2015), no. 2 025041, [[arXiv:1503.02498](#)].
- [16] M. Mondello and N. Goldenfeld, *Scaling and vortex dynamics after the quench of a system with a continuous symmetry*, *Phys. Rev.* **A42** (1990) 5865–5872.

- [17] A. J. Bray, *Theory of phase-ordering kinetics*, *Advances in Physics* **43** (May, 1994) 357–459, [[cond-mat/9501089](#)].
- [18] T. W. B. Kibble, *Topology of Cosmic Domains and Strings*, *J. Phys.* **A9** (1976) 1387–1398.
- [19] A. Vilenkin, *Cosmic Strings and Domain Walls*, *Phys. Rept.* **121** (1985) 263–315.
- [20] N. Turok, *Global Texture as the Origin of Cosmic Structure*, *Phys. Rev. Lett.* **63** (1989) 2625.